Local Nearest Neighbor Integrity Risk Evaluation for Robot Navigation

Guillermo Duenas Arana¹, Mathieu Joerger², Member, IEEE, and Matthew Spenko¹, Member, IEEE

Abstract—This paper describes the design of a new integrity risk prediction/monitoring methodology for robot localization that uses feature extraction and data association algorithms. The work specifically addresses incorrect association faults when employing a local nearest neighbor data association algorithm. This approach is more efficient and easier to implement than previous work. The methodology is tested in simulation, showing that the computed upper bound on integrity risk is a performance metric capable of providing warnings when the safety of the system cannot be guaranteed.

I. Introduction

Pose estimation performance is typically quantified using a covariance matrix or particle spread [1], [2], but this is insufficient for life- and mission-critical applications, such as self-driving cars and other co-robots [3]. In these situations, ignoring faults can lead to catastrophic localization errors. In response, this work quantifies the safety risk involved with data association faults by calculating the system's navigation integrity risk, or the probability that a robot's pose estimate lies within pre-defined limits [4].

Several methods can predict integrity risk in GPS-based aviation applications, but cannot be directly applied to robots that operate in GPS-denied environments [5], [6]. Thus, methods must be developed that account for the faults present in additional sensors, such as lidar. In this regard, there has been relatively little work and none present practical safety levels or rigorous proof of integrity [7], [8], [9].

The authors' prior work established an integrity monitor for lidar-based localization using an EKF coupled with the Global Nearest Neighbor (GNN) data association algorithm [10], [11]. However, the computational complexity of the GNN limits applicability to on-line implementation. In response, this paper extends prior derivations to the more efficient and easily implemented Local Nearest Neighbor (LNN) method as well as deriving a closer bound when allocating integrity risk.

In this paper, Section II provides a mathematical background. Section III bounds the probability of correct association, used in calculating integrity risk. The complete integrity bounding process is presented in Section III-E for ease of implementation. Simulation results are given in Section IV. Finally, Section V presents conclusions and future work.

II. BACKGROUND

This section introduces the necessary mathematical notation and presents the data association criteria employed in this paper.

A. Measurement Model

Measurements corresponding to extracted feature i are stacked in the $m_F \times 1$ vector \mathbf{z}_i . To lighten notations, no time index is specified unless noted otherwise. A landmark map is comprised of n_L landmarks from which n_F features are extracted ($n_F <<< n_L$, typically). We assume all mapped landmarks are the same type and all features provide the same number of measurements, m_F . The landmark from which feature i has been extracted is denoted i_t ; the feature extracted from landmark t is denoted i_t .

The measurement model for a single extracted feature is:

$$\mathbf{z}_i = \mathbf{h}_{t_i}(\mathbf{x}) + \mathbf{v}_i \tag{1}$$

where $\mathbf{h}_t(\cdot)$ is the measurement model function of landmark t, \mathbf{x} is the unknown state vector containing the robot pose, and \mathbf{v}_i is the sensor noise corresponding to feature i's measurements. We assume white Gaussian sensor noise where \mathbf{V}_i is the measurement noise covariance matrix for feature i:

$$\mathbf{v}_i \sim \mathcal{N}\left(\mathbf{0}, \mathbf{V}_i\right)$$
 (2)

B. Innovation Vector

The difference between a feature's measurements and the expected measurements from a landmark is the innovation. Small innovations are indicative of correct associations. The innovation vector of feature i and landmark t is:

$$\gamma_{i,t} = \mathbf{z}_i - \mathbf{h}_t(\bar{\mathbf{x}}) \tag{3}$$

where the state vector after the EKF prediction step $\bar{\mathbf{x}}$ is normally distributed with mean \mathbf{x} and covariance matrix $\bar{\mathbf{P}}$:

$$\bar{\mathbf{x}} \sim \mathcal{N}\left(\mathbf{x}, \bar{\mathbf{P}}\right)$$
 (4)

Substituting (1) into (3) and linearizing using a first order Taylor expansion [10] yields:

$$\gamma_{i,t} \approx \mathbf{y}_{t,t} + \mathbf{H}_t \bar{\epsilon} + \mathbf{v}_i$$
 (5)

where $\mathbf{y}_{t_i,t} \triangleq \mathbf{h}_{t_i}(\mathbf{x}) - \mathbf{h}_t(\mathbf{x})$ is the innovation's faulted vector, $\mathbf{H}_t \triangleq \frac{\partial \mathbf{h}_t(\mathbf{x})}{\partial \mathbf{x}}\Big|_{\bar{\mathbf{x}}}$ is the Jacobian of the measurement model function for landmark t and, $\bar{\boldsymbol{\epsilon}} \triangleq \mathbf{x} - \bar{\mathbf{x}}$ is the prediction estimate error. From (5), the innovations are normally distributed as:

$$\gamma_{i,t} \sim \mathcal{N}\left(\mathbf{y}_{t_i,t}, \mathbf{Y}_{i,t}\right)$$
 (6)

^{*}This work was supported by NSF Grant #1637899.

¹G. Arana and M. Spenko are with the Mechanical, Materials and Aerospace Engineering Dept., Illinois Institute of Technology, Chicago, IL, USA gdueasar@hawk.iit.edu.

²M. Joerger is with the Dept. of Aerospace and Mechanical Engineering, University of Arizona, Tucson, AZ, USA

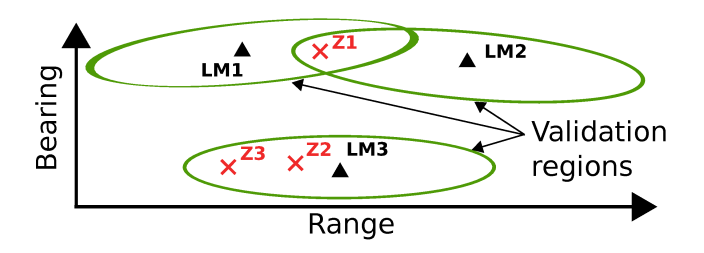


Fig. 1. Range and bearing measurement space for the example in Section II-C. The landmarks are denoted LM1, LM2, and LM3. The features derived from actual measurements are Z1, Z2 and Z3.

where $\mathbf{Y}_{i,t} \triangleq \mathbf{H}_t \bar{\mathbf{P}} \mathbf{H}_t^T + \mathbf{V}_i$. We also define the square of the Innovation weighted Norm (IN) as:

$$\|\boldsymbol{\gamma}_{i,t}\|_{\mathbf{Y}_{i,t}^{-1}}^{2} \triangleq \boldsymbol{\gamma}_{i,t}^{T} \mathbf{Y}_{i,t}^{-1} \boldsymbol{\gamma}_{i,t}$$
 (7)

In general, the square of the IN is noncentral chi-squared distributed with m_F degrees of freedom:

$$\|\boldsymbol{\gamma}_{i,t}\|_{\mathbf{Y}_{i,t}^{-1}}^{2} \sim \chi_{m_{F},\|\boldsymbol{y}_{t_{i},t}\|_{\mathbf{Y}_{i,t}^{-1}}^{2}}^{2}$$
(8)

where $\chi_{a,b}^2$ denotes the noncentral chi-squared distribution with a degrees of freedom and noncentrality parameter b. The INs' particular distribution depends on the correctness of the association. In a correct association, where $t=t_i$, feature i has been extracted from landmark t and thus, the innovation is zero mean, i.e. $\mathbf{y}_{t_i,t} = \mathbf{h}_{t_i}(\mathbf{x}) - \mathbf{h}_t(\mathbf{x}) = \mathbf{0}$, and the IN squared is central chi-squared. In an incorrect association, $t \neq t_i$, feature i has not been extracted from landmark t and thus, the innovation is not zero mean, i.e. $\mathbf{y}_{t_i,t} \neq \mathbf{0}$, and the square of the IN is noncentral chi-squared.

The next section shows how the local nearest neighbor algorithm employs the innovation norms as a data association criteria.

C. Local Nearest Neighbor (LNN)

This section explains the LNN data association criteria using a three-landmark example. The LNN associates each feature with at most one landmark only if the feature is inside the landmark's validation region, comprised of those measurements for which the IN between a feature and a landmark is lower than a predefined threshold T, whose designation is beyond the scope of this work. If the measurement noise covariance matrices are equal for all features, i.e. $\mathbf{V}_i = \mathbf{V}_j \ \forall ij$, the validation regions are also the same for all features. Fig. 1 shows the ellipsoidal validation region boundaries for each landmark assuming equal measurement noise covariance matrices. The LNN data association is thus implemented in the following three steps:

Step 1) Create the $n_F \times n_L$ association matrix with the IN values for every possible association $\|\gamma_{i,t}\|_{\mathbf{Y}_{i,t}^{-1}}$.

Step 2) Remove the associations where the IN is higher

than a threshold T. From Fig. 1:

$$\begin{bmatrix}
LM1 & LM2 & LM3 \\
Z1 & \|\mathbf{\gamma}_{1,1}\|_{\mathbf{Y}_{1,1}^{-1}} & \|\mathbf{\gamma}_{1,2}\|_{\mathbf{Y}_{1,2}^{-1}} & - \\
- & - & \|\mathbf{\gamma}_{2,3}\|_{\mathbf{Y}_{2,3}^{-1}} \\
- & - & \|\mathbf{\gamma}_{3,3}\|_{\mathbf{Y}_{3,3}^{-1}}
\end{bmatrix} (9)$$

where "—" indicates that such association is not validated.

Step 3) Associate each feature with the landmark that results in the smallest validated IN. If a feature has no validated associations, do not associate the feature. Then, the selected association is: $\{Z1 \rightarrow LM1, Z2 \rightarrow LM3, Z3 \rightarrow LM3\}$. This data association criteria may result in multiple associations to the same landmark, as in this example. This is obviously incorrect, but is dealt with in Section III.

This section presented the local nearest neighbor data association that will be used to derive the probability of incorrect association. The next section defines the integrity risk and derives a bound that can be efficiently computed.

D. Hazardous Misleading Information (HMI)

Integrity risk is defined as the probability of Hazardous Misleading Information (HMI). HMI occurs when undetected faults produce unacceptable estimate errors. Exact calculation of the probability of HMI is intractable, instead we derive a computationally efficient analytical upper-bound. The HMI at time k is given as:

$$HMI_k \triangleq \boldsymbol{\alpha}^T \hat{\boldsymbol{\epsilon}}_k > l \tag{10}$$

where α is an $m_F \times 1$ vector that selects the state of interest (or the linear combination of states), $\hat{\epsilon}_k = \mathbf{x}_k - \hat{\mathbf{x}}_k$ is the EKF update estimate error and, l is the acceptable error limit.

The critical difference between this work and a more traditional approach is that we account for incorrect associations (IA) between features and landmarks. Thus, probability of HMI or integrity risk must be evaluated under fault-free, $\neg IA_K$, and faulted, IA_K , conditions, i.e.:

$$P(HMI_k) = P(HMI_k \cap \neg IA_K) + P(HMI_k \cap IA_K)$$
(11)

where a capital letter time subscript denotes all time up to and including such time. An upper bound on the HMI probability, $\check{P}(HMI_k) \geq P(HMI_k)$, is obtained from (11):

$$\check{P}(HMI_k) = 1 + (P(HMI_k \mid \neg IA_K) - 1) \, \check{P}(\neg IA_K) \tag{12}$$

where $P(\neg IA_K) \leq P(\neg IA_K)$ [10].

Equation (12) is used to evaluate the safety risk throughout the rest of the paper. To solve it we must compute $P(HMI_k \mid \neg IA_K)$ and $\check{P}(\neg IA_K)$. The former term denotes the fault-free integrity risk and can be computed using the variance of the state of interest:

$$P(HMI_k \mid \neg IA_K) = P(\boldsymbol{\alpha}^T \hat{\boldsymbol{\epsilon}}_k > l \mid \neg IA_K) = 2\Phi \left[-\frac{l}{\hat{\sigma}_k} \right]$$
(13)

where $\Phi[\cdot]$ is the standard normal CDF and $\hat{\sigma}_k = \sqrt{\alpha^T \hat{\mathbf{P}}_k \alpha}$. An expression of the later, $\check{P}(\neg IA_K)$ (the bound on the probability of correct association), is derived next.

III. CORRECT ASSOCIATION PROBABILITY

This section lower bounds the probability of correctly associating features and landmarks up to, and including time k. The probability of correct association can be recursively evaluated as follows:

$$\breve{P}(\neg IA_K) = \breve{P}(\neg IA_k \mid \neg IA_{K-1})\breve{P}(\neg IA_{K-1}) \tag{14}$$

where $\breve{P}(\neg IA_k \mid \neg IA_{K-1}) \leq P(\neg IA_k \mid \neg IA_{K-1})$ and $\breve{P}(\neg IA_0) = 1$. Thus, only $\breve{P}(\neg IA_k \mid \neg IA_{K-1})$ must be evaluated at each epoch k.

First, we analyze the events that result in an IA. Using the LNN, an IA occurs when A) a feature i is in the validation region of a non-corresponding landmark t ($\neq t_i$) and B) the IN for such landmark t ($\neq t_i$) is the smallest among all INs resulting from feature i. Then:

$$P(IA_{k} \mid \neg IA_{K-1}) \leq P\left(\bigcup_{i} \bigcup_{t \neq t_{i}} \left\{ \underbrace{\|\boldsymbol{\gamma}_{i,t}\|_{\boldsymbol{Y}_{i,t}^{-1}} < T}_{A} \right. \cap \left. \underbrace{\left[\bigcap_{l \neq t} \|\boldsymbol{\gamma}_{i,t}\|_{\boldsymbol{Y}_{i,t}^{-1}} < \|\boldsymbol{\gamma}_{i,l}\|_{\boldsymbol{Y}_{i,l}^{-1}}\right]}_{B} \right\} \right)$$
(15)

where each term is marked with the letter corresponding to its event (A,B). The next two sections analyze these two events and upper bound their probabilities.

A. Evaluation of Term A

Event A occurs when the IN of an incorrect association is smaller than the validation threshold, T. Then, for any i and any $t \neq t_i$, event A occurs if:

$$\|\boldsymbol{\gamma}_{i,t}\|_{\mathbf{Y}_{i,t}^{-1}} < T \tag{16}$$

Substituting equation (5) into (16):

$$\left\| \mathbf{y}_{t_{i},t} + \mathbf{H}_{t}\bar{\boldsymbol{\epsilon}} + \mathbf{v}_{i} \right\|_{\mathbf{Y}_{i,t}^{-1}} < T \tag{17}$$

We define $\mathbf{M}_t \triangleq \begin{bmatrix} \mathbf{H}_t & \mathbf{I} \end{bmatrix}$ and $\mathbf{r}_i \triangleq \begin{bmatrix} \bar{\boldsymbol{\epsilon}} \\ \mathbf{v}_i \end{bmatrix}$. From (2) and (4):

$$\mathbf{r}_{i} \sim \mathcal{N}(\mathbf{0}, \mathbf{R}_{i})$$
 where $\mathbf{R}_{i} = \begin{bmatrix} \bar{\mathbf{P}} & \mathbf{0} \\ \mathbf{0} & \mathbf{V}_{i} \end{bmatrix}$ (18)

We bound the probability of the event A in (17) as:

$$P\left(\left\|\mathbf{y}_{t_{i},t} + \mathbf{M}_{t}\mathbf{r}_{i}\right\|_{\mathbf{Y}_{i,t}^{-1}} \leq T\right)$$

$$\leq P\left(\left\|\mathbf{y}_{t_{i},t}\right\|_{\mathbf{Y}_{i,t}^{-1}} - \left\|\mathbf{M}_{t}\mathbf{r}_{i}\right\|_{\mathbf{Y}_{i,t}^{-1}} \leq T\right)$$

$$\leq P\left(\left\|\mathbf{y}_{t_{i},t}\right\|_{\mathbf{Y}_{i,t}^{-1}} - T \leq \left\|\mathbf{q}_{i}\right\|\right)$$
(19)

where:

$$\mathbf{q}_{i} \triangleq \mathbf{R}_{i}^{-1/2} \mathbf{r}_{i} \sim \mathcal{N}\left(\mathbf{0}, \mathbf{I}\right) \tag{20}$$

and $\|\mathbf{q}_i\| \geq \|\mathbf{M}_t \mathbf{r}_i\|_{\mathbf{Y}_{i,t}^{-1}}$. More details can be found in [10], [11]. Note that the current derivation differs from the one in [10], [11] in that $\|\mathbf{q}_i\|$ depends on the feature index.

B. Evaluation of Term B

Event B occurs when the IN of an IA is the smallest among all INs of a certain feature. Then, for any feature i and any landmark $t \neq t_i$, event B occurs if:

$$\bigcap_{l \neq t} \| \boldsymbol{\gamma}_{i,t} \|_{\mathbf{Y}_{i,t}^{-1}} < \| \boldsymbol{\gamma}_{i,l} \|_{\mathbf{Y}_{i,l}^{-1}}$$
(21)

and thus, it must be true that:

$$\|\boldsymbol{\gamma}_{i,t}\|_{\mathbf{Y}_{i,t}^{-1}} < \|\boldsymbol{\gamma}_{i,t_i}\|_{\mathbf{Y}_{i,t}^{-1}}$$
 (22)

Following a similar derivation to the evaluation of term A, we can bound the probability of event B using (22) as:

$$P\left(\|\mathbf{\gamma}_{i,t}\|_{\mathbf{Y}_{i,t}^{-1}} < \|\mathbf{\gamma}_{i,t_{i}}\|_{\mathbf{Y}_{i,t_{i}}^{-1}}\right)$$

$$\leq P\left(\|\mathbf{y}_{t_{i},t}\|_{\mathbf{Y}_{i,t}^{-1}} - \|\mathbf{M}_{t}\mathbf{r}_{i}\|_{\mathbf{Y}_{i,t}^{-1}} < \|\mathbf{M}_{t_{i}}\mathbf{r}_{i}\|_{\mathbf{Y}_{i,t_{i}}^{-1}}\right)$$

$$\leq P\left(\|\mathbf{y}_{t_{i},t}\|_{\mathbf{Y}_{i,t}^{-1}} < \|\mathbf{M}_{t}\mathbf{r}_{i}\|_{\mathbf{Y}_{i,t}^{-1}} + \|\mathbf{M}_{t_{i}}\mathbf{r}_{i}\|_{\mathbf{Y}_{i,t_{i}}^{-1}}\right)$$

$$\leq P\left(\frac{1}{2}\|\mathbf{y}_{t_{i},t}\|_{\mathbf{Y}_{i,t}^{-1}} < \|\mathbf{q}_{i}\|\right)$$
(23)

Events A and B were bounded with expressions that can be computed if the mean IN, $\|\mathbf{y}_{t_i,t}\|_{\mathbf{Y}_{i,t}^{-1}}$ is known. The next section upper bounds the probability in (15), which can be efficiently evaluated without knowledge of the mean IN.

C. Bound on the Correct Association Probability

This section incorporates the probabilistic bounds from the previous two sections and eliminates the need to explicitly identify the mean IN to further lower bound the probability of correct association.

1) Events A & B: First, we substitute the probability bounds of events A in (19) and event B in (23) into (15) and bound the probability of the union for a summation:

$$P(IA_{k} \mid \neg IA_{K-1}) \leq \sum_{i=1}^{n_{F}} P\left(\bigcup_{t \neq t_{i}} \left\| \mathbf{y}_{t_{i},t} \right\|_{\mathbf{Y}_{i,t}^{-1}} - T \leq \left\| \mathbf{q}_{i} \right\|\right)$$

$$\bigcap \frac{1}{2} \left\| \mathbf{y}_{t_{i},t} \right\|_{\mathbf{Y}_{i,t}^{-1}} < \left\| \mathbf{q}_{i} \right\|$$
(24)

In this expression, the only random variable is $\|\mathbf{q}_i\|$, which is independent of the landmark index t. Therefore, we can substitute the remaining union with a minimum over all non-corresponding landmarks $(t \neq t_i)$, i.e.:

$$P(IA_{k} \mid \neg IA_{K-1}) \leq \sum_{i=1}^{n_{F}} P\left(\min_{t \neq t_{i}} \left\| \mathbf{y}_{t_{i},t} \right\|_{\mathbf{Y}_{i,t}^{-1}} - T \leq \left\| \mathbf{q}_{i} \right\|\right)$$

$$\bigcap_{t \neq t_{i}} \frac{1}{2} \left\| \mathbf{y}_{t_{i},t} \right\|_{\mathbf{Y}_{i,t}^{-1}} < \left\| \mathbf{q}_{i} \right\|$$

$$\leq \sum_{i=1}^{n_{F}} P\left(\min \left\{ \min_{t \neq t_{i}} \left\| \mathbf{y}_{t_{i},t} \right\|_{\mathbf{Y}_{i,t}^{-1}} - T, \right.\right.$$

$$\min_{t \neq t_{i}} \frac{1}{2} \left\| \mathbf{y}_{t_{i},t} \right\|_{\mathbf{Y}_{i,t}^{-1}} \right\} < \left\| \mathbf{q}_{i} \right\|$$

$$(25)$$

We simplify the expression by only considering the second term in the brackets, which is usually the most restrictive. After which, squaring both sides yields:

$$P(IA_k \mid \neg IA_{K-1}) \le \sum_{i=1}^{n_F} P\left(\min_{t \ne t_i} \frac{1}{4} \left\| \mathbf{y}_{t_i, t} \right\|_{\mathbf{Y}_{i, t}^{-1}}^2 < \left\| \mathbf{q}_i \right\|^2\right)$$
(26)

From (26), the correct association probability is:

$$P(\neg IA_{k} \mid \neg IA_{K-1}) = 1 - P(IA_{k} \mid \neg IA_{K-1}) \ge 1 - n_{F} + \sum_{i=1}^{n_{F}} P\left(\|\mathbf{q}_{i}\|^{2} < \min_{t \neq t_{i}} \frac{1}{4} \|\mathbf{y}_{t_{i},t}\|_{\mathbf{Y}_{i,t}}^{2}\right)$$
(27)

From (20), we know that $\|\mathbf{q}_i\|^2 \sim \chi^2_{m+m_F}$. Thus, the only missing terms in (27) are the mean INs, $\|\mathbf{y}_{t_i,t}\|_{\mathbf{Y}_{-1}^{-1}}$.

2) Mean Innovation's Norm: Exact knowledge of $\|\mathbf{y}_{t_i,t}\|_{\mathbf{Y}_{i,t}^{-1}}$ is not necessary to bound the probability in (27). A lower bound on the minimum mean IN will be employed instead. In order to lighten notation, we define:

$$\|\mathbf{y}_{t_i}\|_{\mathbf{Y}_i^{-1}} \triangleq \min_{t \neq t_i} \|\mathbf{y}_{t_i,t}\|_{\mathbf{Y}_{i,t}^{-1}}$$
 (28)

The lower bound on the minimum mean IN, $\|\mathbf{y}_{t_i}^*\|_{\mathbf{Y}_i^{-1}}$, is obtained such that it bounds the actual minimum mean IN, $\|\mathbf{y}_{t_i}\|_{\mathbf{Y}^{-1}}$, with preallocated probability $I_{\mathbf{y}_i}$, i.e.:

$$P\left(\left\|\mathbf{y}_{t_{i}}\right\|_{\mathbf{Y}_{i}^{-1}} < \left\|\mathbf{y}_{t_{i}}^{*}\right\|_{\mathbf{Y}_{i}^{-1}}\right) \le I_{\mathbf{y}_{i}} \tag{29}$$

where I_{y_i} is a fraction of the total integrity risk allocation for the bounding of the minimum mean INs of all extracted features, I_{y} , which is set to a very low value, e.g. 10^{-10} .

The terms inside the summation in (27) can be lower bounded using $\|\mathbf{y}_{t_i}^*\|_{\mathbf{Y}_i^{-1}}$ and accounting for the integrity risk allocation. First, we rewrite each term as:

$$P\left(\|\mathbf{q}_{i}\|^{2} < \frac{1}{4} \|\mathbf{y}_{t_{i}}\|_{\mathbf{Y}_{i}^{-1}}^{2}\right)$$

$$= P\left(\|\mathbf{q}_{i}\|^{2} < \frac{1}{4} \|\mathbf{y}_{t_{i}}\|_{\mathbf{Y}_{i}^{-1}}^{2} \cap \|\mathbf{y}_{t_{i}}^{*}\|_{\mathbf{Y}_{i}^{-1}} \leq \|\mathbf{y}_{t_{i}}\|_{\mathbf{Y}_{i}^{-1}}\right) + P\left(\|\mathbf{q}_{i}\|^{2} < \frac{1}{4} \|\mathbf{y}_{t_{i}}\|_{\mathbf{Y}_{i}^{-1}}^{2} \cap \|\mathbf{y}_{t_{i}}^{*}\|_{\mathbf{Y}_{i}^{-1}} > \|\mathbf{y}_{t_{i}}\|_{\mathbf{Y}_{i}^{-1}}\right)$$

$$(30)$$

Then, we bound the second term by 0, rewrite the first term using conditional probabilities and substitute (29) into (30):

$$P\left(\|\mathbf{q}_{i}\|^{2} < \frac{1}{4} \|\mathbf{y}_{t_{i}}\|_{\mathbf{Y}_{i}^{-1}}^{2}\right)$$

$$\geq P\left(\|\mathbf{q}_{i}\|^{2} < \frac{1}{4} \|\mathbf{y}_{t_{i}}\|_{\mathbf{Y}_{i}^{-1}}^{2} \mid \|\mathbf{y}_{t_{i}}^{*}\|_{\mathbf{Y}_{i}^{-1}}^{2} \leq \|\mathbf{y}_{t_{i}}\|_{\mathbf{Y}_{i}^{-1}}\right)$$

$$P\left(\|\mathbf{y}_{t_{i}}^{*}\|_{\mathbf{Y}_{i}^{-1}} \leq \|\mathbf{y}_{t_{i}}\|_{\mathbf{Y}_{i}^{-1}}\right)$$

$$\geq P\left(\|\mathbf{q}_{i}\|^{2} < \frac{1}{4} \|\mathbf{y}_{t_{i}}^{*}\|_{\mathbf{Y}_{i}^{-1}}^{2}\right) P\left(\|\mathbf{y}_{t_{i}}^{*}\|_{\mathbf{Y}_{i}^{-1}} \leq \|\mathbf{y}_{t_{i}}\|_{\mathbf{Y}_{i}^{-1}}\right)$$

$$\geq X_{m+m_{F}}^{2} \left[\frac{1}{4} \|\mathbf{y}_{t_{i}}^{*}\|_{\mathbf{Y}_{i}^{-1}}^{2}\right] \left(1 - I_{\mathbf{y}_{i}}\right)$$
(31)

where $X_a^2[\cdot]$ is a chi-squared CDF with a degrees of freedom.

3) Bound definition: The probability of correct association at time k can be bounded by substituting (31) into (27):

$$\check{P}(\neg IA_k \mid \neg IA_{K-1}) \triangleq 1 - n_F + \left(1 - \frac{I_{\mathbf{y}}}{n_F}\right) \sum_{i=1}^{n_F} X_{m+m_F}^2 \left[\frac{1}{4} \left\|\mathbf{y}_{t_i}^*\right\|_{\mathbf{Y}_i^{-1}}^2\right] \quad (32)$$

where $I_y = n_F I_{y_i}$ is equally allocated among all features. We substitute (32) into (14) to recursively obtain $\check{P}(\neg IA_K)$.

This section lower bounded the probability of correct association using a lower bound of the minimum mean IN. Next, we derive an analytical expression for $\|\mathbf{y}_{t_i}^*\|_{\mathbf{Y}^{-1}}$.

D. Mean Innovation's Norm Bound

In this section, the minimum mean IN is bounded for a given pose estimate and map of landmarks, but prior to obtaining sensor measurements.

We bound the mean IN of every landmark pair in the extended Field of View (FoV), defined as the region around the robot's positioning estimate within:

$$r_{FoV} = r_{max} - \lambda_{FoV} \Phi^{-1} \left[\frac{I_{FoV}}{2m_{xyz}} \right]$$
 (33)

where r_{max} is the sensor range, λ_{FoV}^2 is the maximum eigenvalue of the covariance matrix elements corresponding to the robot's position, $\Phi^{-1}[\cdot]$ denotes the standard normal CDF, m_{xyz} is the number of states for positioning only (e.g. two in a plane), and I_{FoV} is an integrity risk allocation. I_{FoV} accounts for cases where the extended FoV does not enclose all landmarks in the actual FoV of the robot and will be subtracted from (32). Thus, given the EKF estimate prediction $\bar{\mathbf{x}}$ at time k (not indicated here), we define:

$$\bar{\mathbf{y}}_{l,t} \triangleq \mathbf{h}_l(\bar{\mathbf{x}}) - \mathbf{h}_t(\bar{\mathbf{x}}) \tag{34}$$

which can be linearized as:

$$\bar{\mathbf{y}}_{l,t} \approx \mathbf{h}_{l}(\mathbf{x}) + \mathbf{H}_{l}\bar{\boldsymbol{\epsilon}} - (\mathbf{h}_{t}(\mathbf{x}) + \mathbf{H}_{t}\bar{\boldsymbol{\epsilon}})
\approx \mathbf{h}_{l}(\mathbf{x}) - \mathbf{h}_{t}(\mathbf{x}) + (\mathbf{H}_{l} - \mathbf{H}_{t})\bar{\boldsymbol{\epsilon}}
\approx \mathbf{y}_{l\,t} + (\mathbf{H}_{l} - \mathbf{H}_{t})\bar{\boldsymbol{\epsilon}}$$
(35)

and, from (35):

$$\bar{\mathbf{y}}_{l,t} \sim \mathcal{N}\left(\mathbf{y}_{l,t}, \underbrace{\left(\mathbf{H}_{l} - \mathbf{H}_{t}\right)\bar{\mathbf{P}}\left(\mathbf{H}_{l} - \mathbf{H}_{t}\right)^{T}}_{\triangleq \mathbf{M}_{l,t}}\right)$$
(36)

Thus, the weighted norm is distributed as:

$$\|\bar{\mathbf{y}}_{l,t}\|_{\mathbf{M}_{l,t}^{-1}}^{2} \triangleq \bar{\mathbf{y}}_{l,t}^{T} \mathbf{M}_{l,t}^{-1} \bar{\mathbf{y}}_{l,t} \sim \chi_{m_{F},\|\mathbf{y}_{l,t}\|_{\mathbf{M}_{l,t}^{-1}}^{2}}^{2}$$
(37)

In order to lower bound the mean IN, $\|\mathbf{y}_{l,t}\|_{\mathbf{Y}_{i_l,t}^{-1}}$, we use the sample, $\|\bar{\mathbf{y}}_{l,t}\|_{\mathbf{M}_{i_l}^{-1}}$, from (37) and relate both terms as:

$$\|\mathbf{y}_{l,t}\|_{\mathbf{Y}_{l_{l},t}^{-1}}^{2} = \mathbf{y}_{l,t}^{T} \mathbf{Y}_{i_{l},t}^{-1} \mathbf{y}_{l,t}$$

$$= \mathbf{y}_{l,t}^{T} \mathbf{M}_{l,t}^{-1/2} \underbrace{\mathbf{M}_{l,t}^{1/2} \mathbf{Y}_{i_{l},t}^{-1} \mathbf{M}_{l,t}^{1/2}}_{\geq \lambda_{l,t}^{2}} \mathbf{M}_{l,t}^{-1/2} \mathbf{y}_{l,t}$$

$$\geq \lambda_{l,t}^{2} \mathbf{y}_{l,t}^{T} \mathbf{M}_{l,t}^{-1} \mathbf{y}_{l,t}$$

$$\geq \lambda_{l,t}^{2} \|\mathbf{y}_{l,t}\|_{\mathbf{M}_{l},t}^{2}$$

$$\geq \lambda_{l,t}^{2} \|\mathbf{y}_{l,t}\|_{\mathbf{M}_{l},t}^{2}$$
(38)

where $\lambda_{l,t}^2$ is the smallest eigenvalue of $\mathbf{M}_{l,t}^{1/2}\mathbf{Y}_{l,t}^{-1}\mathbf{M}_{l,t}^{1/2}$. Then, the lower bound of each landmark pair is defined as:

$$\|\mathbf{y}_{l,t}^*\|_{\mathbf{Y}_{l,t}^{-1}} \triangleq \lambda_{l,t} \|\mathbf{y}_{l,t}^*\|_{\mathbf{M}_{l,t}^{-1}}$$
 (39)

The lower bound on $\|\mathbf{y}_{l,t}\|_{\mathbf{M}_{l,t}^{-1}}$ is obtained by creating a confidence set:

$$C(\left\|\bar{\mathbf{y}}_{l,t}\right\|_{\mathbf{M}_{l,t}^{-1}}) = \left\{\left\|\mathbf{y}_{l,t}\right\|_{\mathbf{M}_{l,t}^{-1}} : \left\|\mathbf{y}_{l,t}^{*}\right\|_{\mathbf{M}_{l,t}^{-1}} < \left\|\mathbf{y}_{l,t}\right\|_{\mathbf{M}_{l,t}^{-1}}\right\}$$

such that the same integrity risk allocation, $I_{\mathbf{y}_i}$, in (29) is met. Note that the bound, $\left\|\mathbf{y}_{l,t}^*\right\|_{\mathbf{M}_{l,t}^{-1}}$, will be a function of the sample, $\left\|\bar{\mathbf{y}}_{l,t}\right\|_{\mathbf{M}_{l}^{-1}}$. We rewrite this set as:

$$C(\left\|\bar{\mathbf{y}}_{l,t}\right\|_{\mathbf{M}_{l,t}^{-1}}) = \left\{\left\|\mathbf{y}_{l,t}\right\|_{\mathbf{M}_{l,t}^{-1}} : Q_{l,t} < \beta\right\}$$
(41)

where $Q_{l,t} \triangleq \left\| \bar{\mathbf{y}}_{l,t} \right\|_{\mathbf{M}_{l,t}^{-1}} - \left\| \mathbf{y}_{l,t} \right\|_{\mathbf{M}_{l,t}^{-1}}$ To meet equation (29), it must be true that:

$$P\left(Q_{l,t} < \beta\right) > 1 - I_{\mathbf{v}_{s}} \tag{42}$$

or, using a more restrictive condition:

$$P\left(Q_{l,t} < \beta\right) > P\left(Q'_{l,t} < \beta\right) > 1 - I_{\mathbf{y}_i} \tag{43}$$

where $Q'_{l,t} \triangleq \|\bar{\mathbf{y}}_{l,t} - \mathbf{y}_{l,t}\|_{\mathbf{M}_{l,t}^{-1}} \geq Q_{l,t}$ and thus, $(Q'_{l,t})^2 \sim \chi^2_{m_F}$. Then, we can obtain β by equalizing (43):

$$\beta = \sqrt{X_{m_F}^{-2} \left[1 - I_{\mathbf{y}_i} \right]} \tag{44}$$

where $X_a^{-2}[\cdot]$ denotes the chi-squared inverse CDF with a degrees of freedom. Substituting $Q_{l,t}$ and β in (41) and reorganizing terms:

$$C(\|\bar{\mathbf{y}}_{l,t}\|_{\mathbf{M}_{l,t}^{-1}}) = \left\{ \|\mathbf{y}_{l,t}\|_{\mathbf{M}_{l,t}^{-1}} : \|\bar{\mathbf{y}}_{l,t}\|_{\mathbf{M}_{l,t}^{-1}} - \sqrt{X_{m_F}^{-2} \left[1 - I_{\mathbf{y}_i}\right]} < \|\mathbf{y}_{l,t}\|_{\mathbf{M}_{l,t}^{-1}} \right\}$$

$$(45)$$

Comparing (45) with (40), we define:

$$\|\mathbf{y}_{l,t}^*\|_{\mathbf{M}_{l,t}^{-1}} \triangleq \|\bar{\mathbf{y}}_{l,t}\|_{\mathbf{M}_{l,t}^{-1}} - \sqrt{X_{m_F}^{-2} \left[1 - I_{\mathbf{y}_i}\right]}$$
 (46)

Finally, substituting (46) into (39) and taking the minimum over the landmarks in the extended FoV, the lower bound is:

$$\|\mathbf{y}_{l}^{*}\|_{\mathbf{Y}_{i_{l}}^{-1}} \triangleq \min_{\substack{t \in \Omega_{FoV} \\ t \neq l}} \lambda_{l,t} \left(\left\| \bar{\mathbf{y}}_{l,t} \right\|_{\mathbf{M}_{l,t}^{-1}} - \sqrt{X_{m_{F}}^{-2} \left[1 - I_{\mathbf{y}_{i}} \right]} \right)$$

$$(47)$$

where the set Ω_{FoV} includes all landmarks in the extended FoV. Including only the landmarks in the extended FoV defined by (33) results in a lower $\|\mathbf{y}_l^*\|_{\mathbf{Y}_{i_l}^{-1}}$, but directly decreases the bound on the probability of correct association in (32) by I_{FoV} as will be noted in the next section.

This section derived a lower bound on the minimum mean IN that is used to compute the probability of correct association bound. The next section summarizes the complete integrity risk bounding process.

TABLE I SIMULATION PARAMETERS

Std. dev. on lidar range, bearing	$0.3m, 2^{\circ}$
Std. dev. on robot velocity, steering angle	$0.3m/s, 2^{\circ}$
lidar range	25m
lidar sampling interval	0.1s
Alert limit	1m
$I_{\mathbf{y}}$	10^{-10}
I_{FoV}	10^{-12}

E. Summary of Equations

This section presents the equations needed for the computation of the integrity risk bound at time k. The HMI probability or integrity risk is upper bounded as:

$$\check{P}(HMI_k) = 1 + (P(HMI_k) \mid \neg IA_K) - 1) \check{P}(\neg IA_K)$$
(48)

where:

$$P(HMI_k \mid \neg IA_K) = 2\Phi \left[-\frac{l}{\hat{\sigma}_k} \right] \tag{49}$$

$$\check{P}(\neg IA_K) = \prod_{j=1}^k \check{P}(\neg IA_j \mid \neg IA_{J-1}) \tag{50}$$

In order to do integrity prediction, we assume that all landmarks in the FoV, n_{FoV} , are detected. Thus:

$$\check{P}(\neg IA_k \mid \neg IA_{K-1}) = 1 - I_{FoV} - n_{FoV} + \left(1 - \frac{I_{\mathbf{y}}}{n_{FoV}}\right) \sum_{l=1}^{n_{FoV}} X_{m+m_F}^2 \left[\frac{1}{4} \|\mathbf{y}_l^*\|_{\mathbf{Y}_{i_l}^{-1}}^2\right]$$
(51)

where, allocating I_v equally among landmarks:

$$\|\mathbf{y}_{l}^{*}\|_{\mathbf{Y}_{i_{l}}^{-1}} = \min_{\substack{t \in \Omega_{FoV} \\ t \neq l}} \lambda_{l,t} \left(\left\| \bar{\mathbf{y}}_{l,t} \right\|_{\mathbf{M}_{l,t}^{-1}} - \sqrt{X_{m_{F}}^{-2}} \left[1 - \frac{I_{\mathbf{y}}}{n_{FoV}} \right] \right)$$
(52)

$$\mathbf{M}_{l,t} = (\mathbf{H}_l - \mathbf{H}_t) \,\bar{\mathbf{P}} \left(\mathbf{H}_l - \mathbf{H}_t\right)^T \tag{53}$$

$$\lambda_{l,t} = \text{min eigenvalue of } \mathbf{M}_{l,t}^{1/2} \mathbf{Y}_{i_l,t}^{-1} \mathbf{M}_{l,t}^{1/2}$$
 (54)

This section lower bounded the probability of correct association for the LNN data association method specified in Section II-C. The bound is used to calculate the integrity risk bound (Section III-E), which is implemented next.

IV. SIMULATION RESULTS

In this section, a simulated car-like robot follows a straight path with landmarks on both sides (see Fig. 2) to demonstrate the integrity risk bound summarized in Section III-E. Velocity and steering angle are read at every epoch, and a simulated lidar provides range and bearing to point landmarks ($m_F = 2$). All are disturbed with white Gaussian noise (see Table I). An EKF tracks the robot state (x, y, θ) and equations (48)-(54) predict the integrity risk one epoch ahead of the current time. During the first 430m, landmarks are well-spaced with respect to the system uncertainty (30m in both X and Y directions between landmarks). At 430m,

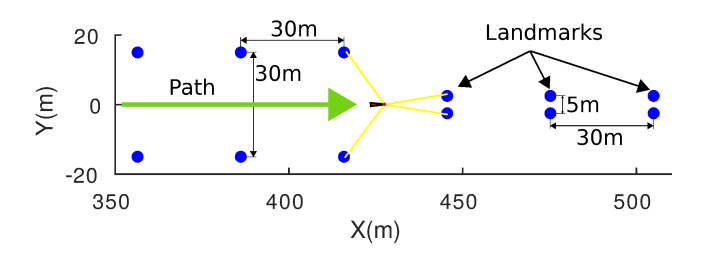


Fig. 2. Robot detecting four landmarks when transitioning between the well spaced and the poorly spaced landmarks. The depicted scenario corresponds to epoch ≈ 300 .

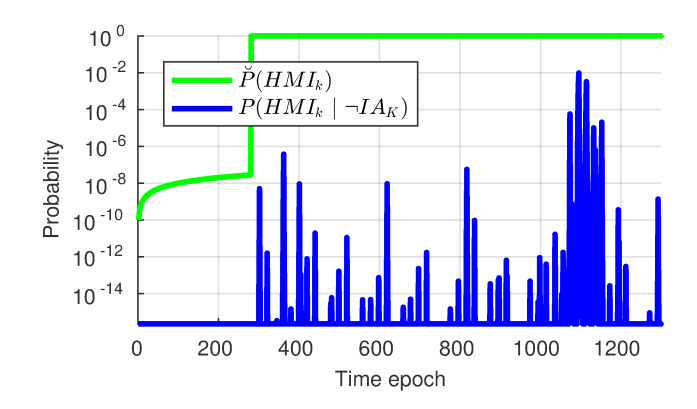


Fig. 3. The HMI probability derived in this work vs. the variance based HMI probability that does not account for faults.

the vertical spacing between landmarks is reduced to only 5m.

The integrity risk bound (green) in Fig. 3 shows two sections. The first, epochs 1–300, corresponds to the well-spaced landmark region where the integrity level required for life-critical operations is ensured, i.e. $P(HMI_k) \leq I_{REQ} = 10^{-7}$. When the robot enters the poorly-spaced landmark section, integrity cannot be guaranteed because of the risk of possible incorrect associations.

Fig. 4 shows the robot's lateral positioning estimate error (red) as well as its 3σ covariance envelope (blue). As in Fig. 3, sections corresponding to the well spaced (epochs 1–300) and the poorly spaced landmarks (epochs 301–end) both exist. Without faults, the 3σ envelope over bounds the estimate error with 0.997 probability, as it is the case when traversing the well spaced landmark region. When IAs occur, the 3σ envelope no longer has to bound the estimate error. For example, multiple IAs arise while traversing the poorly spaced landmark region until HMI occurs at epoch 1080. For the next 100 epochs, the estimated lateral position error is $\approx 5m$ while the 3σ envelope barely reaches 1m. For lifecritical co-robotic applications, this is extremely dangerous. For example, if this robot were a self-driving car, the pose estimate would be in the wrong lane. Thus, the variancebased probability of HMI (blue) in Fig. 3 is not enough to ensure safety when faults occur.

V. CONCLUSIONS & FUTURE WORK

This paper presents a new integrity prediction methodology to ensure localization safety in the presence of faults

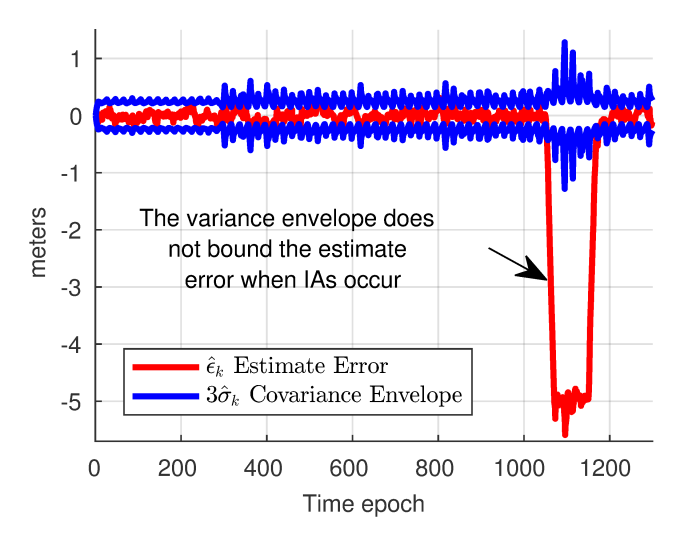


Fig. 4. 3σ covariance envelope vs. estimate error for the state of interest.

caused by the local nearest neighbor data association. The methodology is tested in simulation. The results show that the estimate variance is not a sufficient performance metric and we must assess the risk of faults to ensure safety in life-critical applications.

In future work, we will derive a method to minimize the integrity risk bound by optimizing the I_y and I_{FoV} integrity risk allocations and *a priori* selecting which mapped landmarks to associate. Additionally, the feature extractor system will be analyzed to account for possible extractions of unmapped objects and mis-extractions of mapped landmarks.

REFERENCES

- [1] G. Dissanayake, P. Newman, S. Clark, H. Durrant-Whyte, and M. Csorba, "A Solution to the Simultaneous Localization and Map Building (SLAM) Problem," *IEEE Trans. on Robotics Automation*, vol. 17, no. 3, pp. 229–241, 2001.
- [2] J. Leonard and H. Durrant-Whyte, Directed Sonar Sensing for Mobile Robot Navigation. Kluwer Academic Publishers, 1992.
- [3] N. A. Othman and H. Ahmad, "The analysis of covariance matrix for kalman filter based slam with intermittent measurement," in *Proc. Int. Conf. Systems, Control, and Informatics*, 2013.
- [4] R. T. C. for Aeronautics Special Committee 159, "Minimum Aviation System Performance Standards for the Local Area Augmentation System (LAAS)," Document RTCA/DO-245, 2004.
- [5] R. G. Brown, "A baseline gps raim scheme and a note on the equivalence of three raim methods," *Navigation*, vol. 39, no. 3, pp. 301–316, 1992.
- [6] W. G. C. A. T. Subgroup, "Milestone 3 Report," EU-US Cooperation on Satellite Navigation, Tech. Rep., 2015.
- [7] J. Lee, B. Kim, J. Seo, K. Yi, J. Yoon, and B. Ko, "Automated driving control in safe driving envelope based on probabilistic prediction of surrounding vehicle behaviors," SAE Int. J. Passenger Cars-Electronic and Electrical Systems, vol. 8, no. 2015-01-0314, pp. 207–218, 2015.
- [8] O. Le Marchand, P. Bonnifait, J. Ibañez-Guzmán, and D. Bétaille, "Vehicle localization integrity based on trajectory monitoring," in IEEE/RSJ ICRA. IEEE, 2009, pp. 3453–3458.
- [9] R. Toledo-Moreo, M. A. Zamora-Izquierdo, B. Úbeda-Miñarro, and A. F. Gómez-Skarmeta, "High-integrity imm-ekf-based road vehicle navigation with low-cost gps/sbas/ins," *IEEE Trans. on Intelligent Trans. Systems*, vol. 8, no. 3, pp. 491–511, 2007.
- [10] M. Joerger, M. Jamoom, M. Spenko, and B. Pervan, "Integrity of laser-based feature extraction and data association," in 2016 IEEE/ION PLANS, April 2016, pp. 557–571.
- [11] M. Joerger and B. Pervan, "Quantifying safety of laser-based navigation (submitted)," *IEEE TAES*, 2017.